Electronic Supplementary Material (ESI) for ChemComm.

Creating a hyperpolarised pseudo singlet state through polarisation transfer from *para*hydrogen under SABRE

Alexandra M. Olaru,[‡a] Soumya S. Roy, [‡a] Lyrelle S. Lloyd,[a] Steven Coombes,[b] Gary G. R. Green,[c] and Simon B. Duckett*[a]

1. Experimental

Materials All of the experimental procedures associated with this work were carried out under nitrogen using standard Schlenk techniques. The solvents used were dried using an Innovative Technology anhydrous solvent system, or distilled from an appropriate drying agent under nitrogen. Catalysts were prepared according to literature methods [1]. Deuterated methanol and 2-aminothiazole were obtained from Sigma-Aldrich and used as supplied.

The catalyst precursors ([Ir(IMes)(COD)Cl] and [Ir(SIMes)(COD)Cl]) and ([Ir(IPr)(COD)Cl] were employed . These catalysts were synthesized by established procedures [2]. The SABRE experiments used different concentrations of the substrate and catalyst as detailed below. Deuterated methanol was used as the solvent in all cases (Sigma Aldrich).

Instrumentation and procedures All NMR measurements were recorded on Bruker Avance III series 400 MHz or 500 MHz systems. NMR samples were prepared in 5 mm NMR tubes fitted with Young's valves. Samples were degassed prior to *p*-H_2 (3 bars) addition. The T_{LLS} measurements were performed at 400 MHz as detailed in section 2.7.

NMR characterization data was collected using a range of 1-D and 2-D methods that included nOe, COSY and HMQC procedures [3-7]. The slow dynamic processes exhibited by complexes **3a**-**3c** were studied by EXSY methods [8].

SABRE analysis NMR samples were prepared containing **3a**, **3b** or **3c** in 0.6 ml of methanol-d_4. Arrays of NMR measurements were collected using either 5 or 20 equivalents of substrate to 5 mM of

iridium (leading to samples containing 2- and 17-fold excesses of **atz** relative to iridium, respectively). After adding *p*-H_2 at 3 bar pressure, ^{1}H NMR spectra were recorded using π/2 excitation pulses immediately after shaking the sample in a magnetic field of 65 G. Enhancement factors were calculated by using the ratio of the integral areas of individual resonances in the hyperpolarised spectrum and the spectrum collected under normal H_2 and Boltzmann equilibrium conditions respectively.

Typical samples reflect the following situations:

Sample 1. 3.1 μM IMes catalyst + 0.064 M substrate (making it a 2-fold excess of atz) in 0.6 ml solvent.

Sample 2. 3.1 μM IMes catalyst + 0.25 M substrate (making it a 17-fold excess of atz) in 0.6 ml solvent.

Sample 3. 3.1 μM SIMes catalyst + 0.064 M substrate (making it a 2-fold excess of atz) in 0.6 ml solvent.

Sample 4. 3.1 μM SIMes catalyst + 0.25 M substrate (making it a 17-fold excess of atz) in 0.6 ml solvent.

Field dependence Polarization transfer field (PTF) measurements were recorded using an automated system that allows for repeated hyperpolarisation in the presence of constant low fields of accurate values [9]. Samples containing 10 mg of **3a** and **3b** (5 mM) and 2- and 17-fold excesses of **atz** respectively were prepared in 3 ml of methanol-d_4. After dissolution, the samples were introduced in the flow system and pulse-and-collect, as well as multi-quantum filtered experiments were performed at PTFs that ranged from 0 to 140 G, in steps of 10 G. The external magnetic field was screened by placing the mixing chamber containing the sample and the PTF coil in a mu-metal shield. Details of the polariser have been reported [9].

EXSY measurements and kinetic analysis A series of exchange spectroscopy (EXSY) measurements were made to probe the dynamic behaviour of these systems [3]. This process involved the selective excitation of a single resonance and the subsequent measurement of a ^{1}H NMR spectrum at time, t, after the initial pulse. The resulting measurements consisted of a series of data arrays such that t is varied between 10 and 25 values, typically between 0.1 to 1.0 s, to encode the reaction profile. The precise values were varied with temperature to suit the speed of the process. Data was collected for a range of temperatures and sample concentrations. Integrals for the interchanging peaks in the associated ^{1}H EXSY spectra were obtained and converted into a percentage of the total detected signal.

These data were then analysed as a function of the mixing time according to a differential kinetic model [10]. Rates of exchange were determined by employing a Runge-Kutta [11] scheme to solve the system of differential equations and a Levenberg–Marquardt algorithm [12] to minimize the sum of the residuals in the associated least mean squares analysis. The theoretical model used to fit the experimental EXSY data involved a two-site exchange (A ↔ B), as expressed by the equations below:

$$-\frac{dA}{dt} = -K_{ab} * A + K_{ba} * B$$

$$-\frac{dB}{dt} = +K_{ab} * A - K_{ba} * B$$

An example of typical build-up/decay curves obtained from the integration of the experimental EXSY data, together with the corresponding fitted data is presented in Figure S1.

Thermodynamic parameters were calculated using the exchange rates obtained for a wide range of temperatures (detailed in sections 2.2 and 2.3) and the Eyring-Polanyi equation [13].

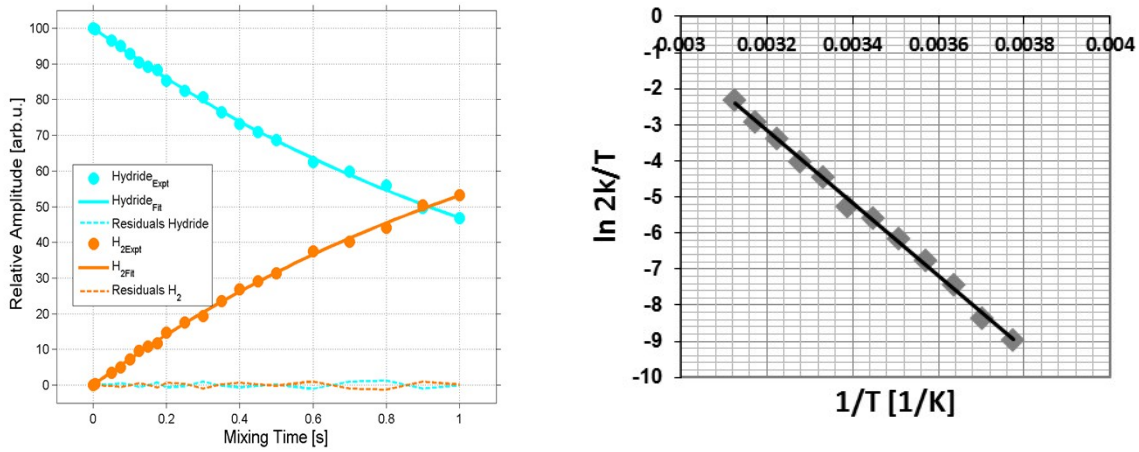

Figure S1: Build-up/decay obtained from the integration of experimental EXSY data recorded for 3a at 295 K (left) and corresponding Eyring plot for the H_2 loss process (right).

2. Experimental Results

2.1 Catalyst effect on SABRE enhancements

Samples containing 5mM concentrations of **3a**, **3b** and **3c** were prepared with a 2-fold excess of substrate and a 17-fold excess of substrate were hyperpolarised as described previously in the experimental section. Up to 7 experiments were performed for each sample and an average enhancement factor was calculated. The results are presented in table T-S1.

The data show that, in both cases, the highest enhancement values are obtained for complex **3b**, followed by **3a** and **3c**. Except for **3c**, lower substrate loading leads to stronger enhancements, as it was also previously shown for other ligands, such as pyridine. In the case of **3c** we assume that a considerable increase in the longitudinal relaxation time is the cause of the increase in polarisation with substrate loading.

Table T-S1. Enhancement vs. catalyst. Individual proton enhancements were calculated as the sum of the total free and bound resonance intensities. H_4 denotes the proton *ortho* to the N atom. The errors were calculated as standard deviations of the population, weighted by limited number of samples.

Complex	Substrate excess (fold)	ε H_4 [arb. u.]	ε H_5 [arb. u.]	ε_{atz} [arb. u.]
3a	2	-654 ± 145	-525 ± 103	-1179 ± 178
	17	-279 ± 28	-189 ± 13	-486 ± 31
3b	2	-901 ± 104	668 ± 57	-1569 ± 119
	17	614 ± 33	-407 ± 23	1022 ± 41
3c	2	-206 ± 17	-58 ± 8	-264 ± 18
	17	-423 ± 49	-178 ± 26	-602 ± 56

2.2 Effect of pressure on hydride loss rate constants

Hydride-H_2 exchange rates were measured for a sample containing **3a** (17-fold excess of **atz**). Experiments were performed on the same sample while varying the H_2 pressure on an interval ranging from 1.5 to 4.0 bar using 0.5 bar increments. Results are presented in figure S2.

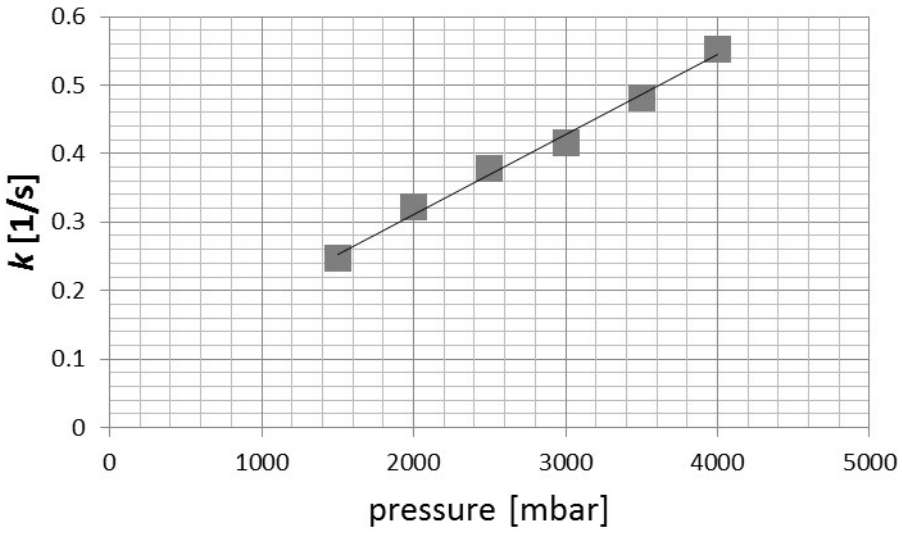

Figure S2: Rate of hydride-H_2 exchange versus H_2 pressure.

Table T-S2 shows the actual rate data as a function of H_2 pressure. It shows that there is a linear increase in the rate of H_2 loss with the increase in H_2 pressure. The process is characterised by the gradient of 0.23 $(s\ bar)^{-1}$.

Table T-S2: Rate of hydride-H_2 exchange versus H_2 pressure.

Pressure [mbar]	k [1/s]
1500	0.247 ± 0.005
2000	0.322 ± 0.01
2500	0.379 ± 0.01
3000	0.415 ± 0.01
3500	0.481 ± 0.01
4000	0.553 ± 0.01

2.3 Catalyst effect on hydride and ligand exchange rates

The rates of ligand and H_2 loss were measured for samples containing **3a**, **3b** and **3c** (17-fold excess of **atz**) on a temperature interval ranging from 260 to 320 K. The relatively high substrate loading ensures that the longitudinal relaxation times of targeted resonances are longer than the time scale of the experiments, such that the effect to T_1 decay during the exchange is negligible. The results are presented in tables T-S3 (H_2 loss) and T-S4 (ligand build-up in solution).

These data show that the H_2 loss is slowest for **3a**, followed by **3b** and **3c**. In the case of **3c**, the exchange with hydrogen occurs so fast that the loss rate could not be measured above room temperature.

The corresponding activation parameters are detailed in Table T-S5 and T-S6. They were obtained by Eyring analysis .

Table T-S3. Rates of H_2 loss as a function of temperature.

T [K]	k_{3a} [1/s]	k_{3b} [1/s]	k_{3c} [1/s]
260	-	-	0.0125 ± 0.0005
265	0.0085 ± 0.0005	0.027 ± 0.001	0.049 ± 0.0025
270	0.016 ± 0.0015	0.0595 ± 0.001	0.135 ± 0.005
275	0.0405 ± 0.001	0.12 ± 0.001	0.28 ± 0.015
280	0.081 ± 0.0005	0.2835 ± 0.0015	0.72 ± 0.005
285	0.1495 ± 0.001	0.509 ± 0.0005	1.35 ± 0.05
290	0.264 ± 0.0015	0.9225 ± 0.004	2.75 ± 0.05
295	0.3795 ± 0.0015	1.75 ± 0.02	5.2 ± 0.1
300	0.855 ± 0.015	3.4 ± 0.015	-
305	1.365 ± 0.03	5.95 ± 0.035	-
310	2.605 ± 0.505	9.3 ± 0.1	-
315	4.15 ± 0.05	-	-
320	7.75 ± 2	-	-
325	10.9 ± 1	-	-

Ligand build-up rates calculated for **3b** are at least twice the ones obtained for **3a**, which could explain the highest enhancement values obtained for the former complex. No experiments were performed on the sample containing **3c**, due to a complete overlap of the free and bound resonances (Table T-S4).

Table T-S4. Ligand build-up rates as a function of temperature.

T [K]	k_{3a} [1/s]	k_{3b} [1/s]	k_{3c} [1/s]
260	-	0.048 ± 0.005	-
265	-	0.069 ± 0.003	-
270	0.034 ± 0.001	0.120 ± 0.002	-
275	0.068 ± 0.001	0.240 ± 0.001	-
280	0.158 ± 0.001	0.530 ± 0.006	-
285	0.321 ± 0.003	0.814 ± 0.004	-
290	0.610 ± 0.005	1.5109 ± 0.007	-
295	1.112 ± 0.004	2.97 ± 0.01	-
300	2.04 ± 0.02	4.7 ± 0.1	-
305	3.47 ± 0.02	7.7 ± 0.2	-
310	5.86 ± 0.03	11.5 ±0.2	-
315	9.0 ± 0.1	-	-

Table T-S5. Activation parameters for H_2 loss.

Activation Parameters	**3a**	**3b**	**3c**
$\Delta H^{\neq}$ (kJ mol^{-1})	83	87.3	105
+/-	2.5	2.3	10
$\Delta S^{\neq}$ (J K^{-1} mol^{-1})	37.3	61.5	133
+/-	8.2	8.0	35
$\Delta G^{\neq}_{300}$ (kJ mol^{-1})	72.2	68.8	65
+/-	1	0.3	9
R Square	0.998	0.998	0.991

Table T-S6. Activation parameters for atz loss.

Activation Parameters	**3a**	**3b**	**3c**
$\Delta H^{\neq}$ (kJ mol^{-1})	86.2	77.2	-
+/-	3.3	2.9	-
$\Delta S^{\neq}$ (J K^{-1} mol^{-1})	54	31	-
+/-	11	10	-
$\Delta G^{\neq}_{300}$ (kJ mol^{-1})	70.1	68.0	-
+/-	1	1	-
R Square	0.997	0.997	-

2.4 Substrate loading effect on enhancement, hydride exchange and ligand build-up rates

SABRE ^{1}H enhancements as well as H_2 and ligand loss rates were measured on a series of samples containing **3a** with 5 mM catalyst concentration and substrate loadings ranging from 4 to 100 equivalents as detailed in Table T-S7.

As shown for other substrates, such as pyridine, the SABRE ^{1}H enhancements factors decrease when the substrate concentration is increased. For **3a** this process follows an exponential trend (Fig. S3) and the total enhancement values decay from -2240 (1-equivalent) to -7.5 (97-fold excess).

As the efficiency of the polarisation transfer process directly depends on the scalar coupling between the ligand's protons and the hydrides, individual protons will have different enhancements, as a function of how close to the binding site they are located in the molecule. The complexity of this process is furthermore increased by the fact that the individual protons also have different relaxation times, so the enhancement obtained will be affected by the rate of signal decay. We have thus considered it informative to report not only the total enhancement obtained per molecule, but also the individual values.

Table- T-S7 Effect of substrate loading on signal enhancement.

Substrate excess (-fold)	ε H_4	ε H_5	ε total
1	-1070 ± 100	-1170 ± 108	-2240 ± 153
3	-890 ± 125	-657 ± 80	-1544 ± 150
5	-860 ± 100	-656 ± 80	1596 ± 135
7	-646 ± 100	-454 ± 70	-1100 ± 119
12	-440 ± 60	-334 ± 50	-774 ± 80
17	-320 ± 40	-209 ± 10	-529 ± 43
37	-74 ± 8	-62 ± 7	-135 ± 10
97	-5 ± 4	3 ± 3	8 ± 5

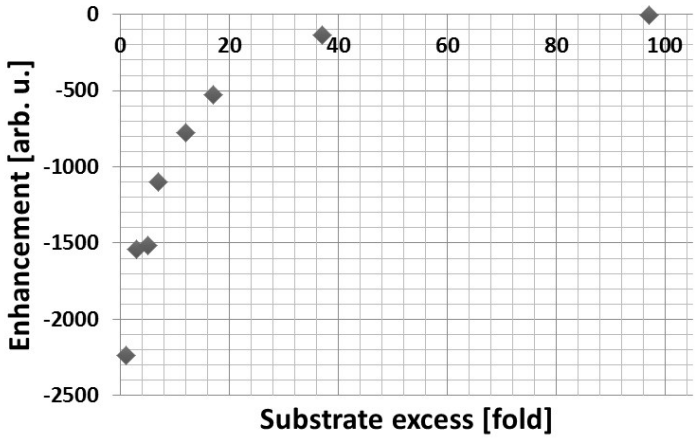

Figure S3: SABRE ^{1}H total enhancement as a function of substrate loading.

The process of H_2 loss becomes considerably slower with increasing ligand concentration. The rates of hydride exchange decrease exponentially from 1.71 s^{-1} (1-fold excess) to 0.27 s^{-1} (97-fold excess). The rate characterising the ligand build-up process is always larger than the H_2 loss rate and is essentially constant irrespective of the substrate concentration (Figure S4 and Table T-S8). This

confirms the dissociative nature of the ligand exchange pathway and the involvement of $[Ir(H)_2(atz)_2(H_2)(NHC)_2]Cl$.

Table T-S8: Raw rate of ligand exchange data as a function of substrate excess for 3b.

Ir : Substrate ratio	H_2 loss rate [1/s]	Ligand build-up rate [1/s]
1:4	0.828 ± 0.003	0.962 ± 0.006
1:6	0.737 ± 0.006	0.907 ± 0.003
1:8	0.719 ± 0.008	0.925 ± 0.001
1:10	0.6505 ± 0.01	0.927 ± 0.001
1:15	0.579 ± 0.007	0.975 ± 0.003
1:20	0.4565 ± 0.008	1.112 ± 0.004
1:30	0.3925 ± 0.005	0.916 ± 0.023
1:40	0.2985 ± 0.005	0.837 ± 0.001
1:60	0.199 ± 0.001	0.864 ± 0.001
1:100	0.1435 ± 0.007	0.675 ± 0.002

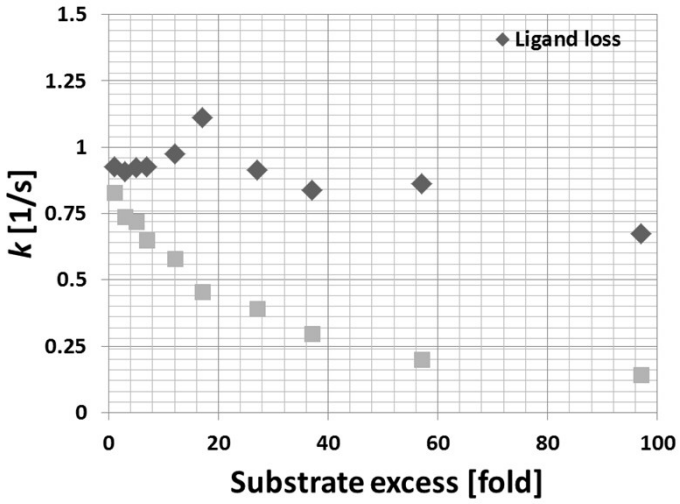

Figure S4: Exchange rates as a function of substrate loading (fold) relative to the 5 mM catalyst concentration.

2.5 Effect of polarisation transfer field on SABRE enhancements

Experiments have been performed using an automated device equipped with a pH_2 delivery system which continuously delivers gas into the polariser which is subsequently transferred into a mixing chamber that contains the sample in solution. The gas is bubbled through the liquid for a defined time in the presence of a coil that produces the local magnetic field required for the polarisation process to take place. After magnetisation transfer occurs, the sample is delivered by the polariser to the high field magnet for detection [9].

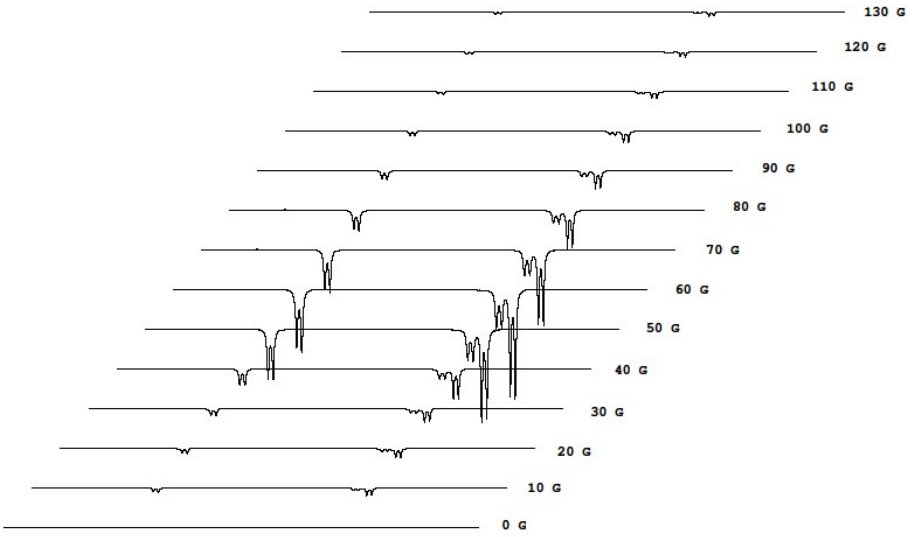

Figure S5: Single scan spectra acquired using PTF values increasing from 0 to 140 G in 10 G increments.

Single scan spectra employing **3a** and **3b** were acquired using hard pulses and gradient based multiple quantum filters at various PTF values as described previously. As for other ligands, the maximum ^1H SABRE enhancement is obtained at approximately 65 G, a field values that matches the J-coupling between the *ortho* resonance and the hydrides (figure S4). Data recorded using zero- and single-quantum filters a similar the same trend for both catalysts (Fig. S5, S6 and S7).

An unusual trend can be observed in the results obtained for **3a** when probing the IS (DQ) terms, as the series of enhancement factors exhibits a local minimum at 40 G and much lower enhancement values at 60 G when compared to 70 G (Fig. S8).

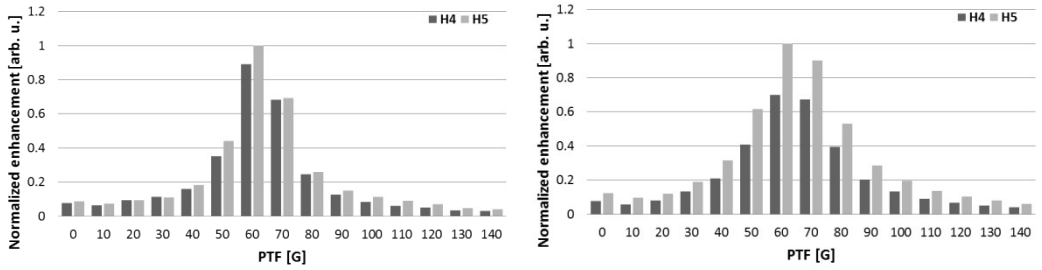

Figure S6: Normalized SABRE ^{1}H individual enhancements for the ZQ terms of 3a (top) and 3b (bottom).

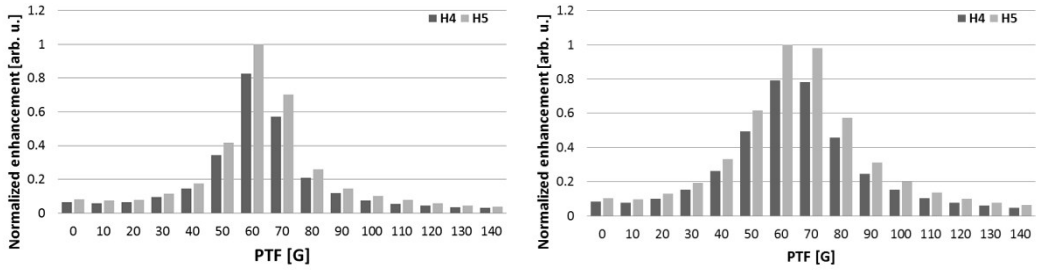

Figure S7: Normalized SABRE ^{1}H individual enhancements for the SQ terms of 3a (top) and 3b (bottom).

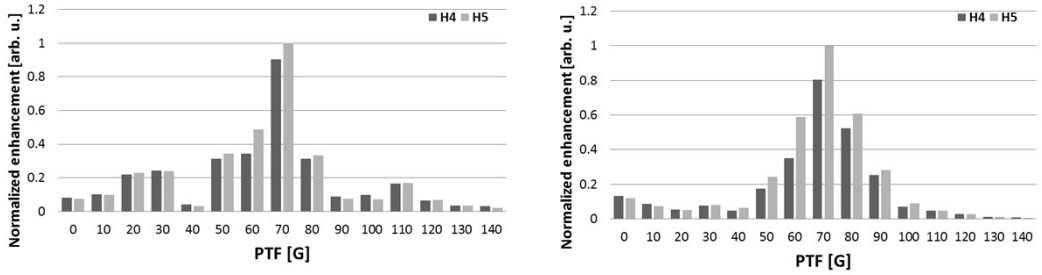

Figure S8: Normalized SABRE ^{1}H individual enhancements for the DQ terms of 3a (top) and 3b (bottom).

2.6 Complex characterisation

A series of NMR spectra were collected to yield the following characterisation data as listed in tables T-S9 to T-S11.

Table T-S9: NMR characterisation data for 3a in MeOD

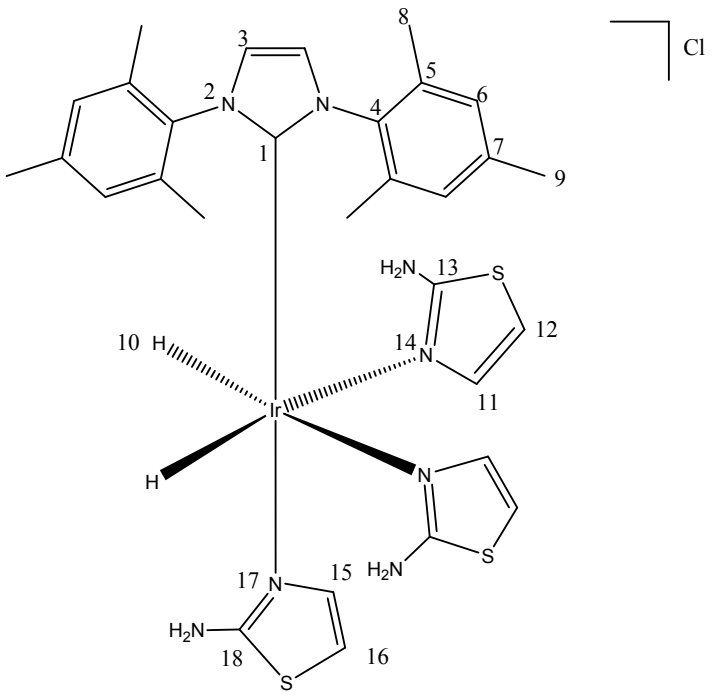

Resonance number	^{1}H (ppm)	^{13}C (ppm)	^{15}N (ppm)
1		150.8	
2			194.45
3	7.13	122.13	
4		137.28	
5		135.0	
6	6.85	128.37	
7		137.9	
8	2.086	17.74	
9	2.287	19.97	
10	-22.76		
11	7.26 d 4.1 Hz	139.5	
12	6.609 d 4.1 Hz	106.0	
13		170.3	
14			183.07
15	6.21 d 4.1 Hz	137.98	
16	5.06 d 4.1 Hz	106.19	
17			172.42
18		168.73	

Table T-S10: NMR characterisation data for 3b in MeOD.

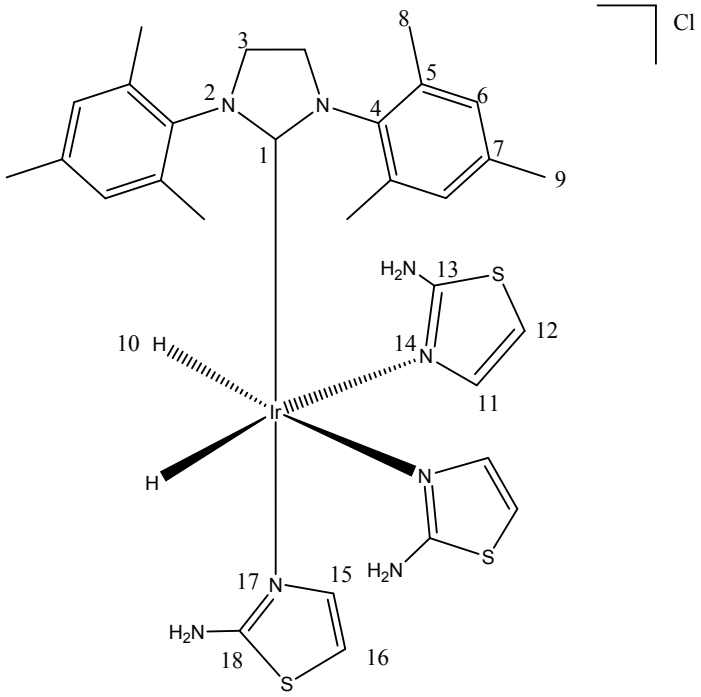

Resonance number	^{1}H (ppm)	^{13}C (ppm)	^{15}N (ppm)
1		137.9	
2			
3	3.85	29.9	
4		137.95	
5		135.75	
6	6.2	128.58	
7		136.77	
8	2.30	17.64	
9	2.25	19.88	
10	-22.75		
11	7.04 d 4.1 Hz	139.55	
12	6.62 d 4.1 Hz	105.92	
13		170.26	
14			183.13
15	6.18 d 4.1 Hz	127.98	
16	5.44 d 4.1 Hz	106.29	
17			174.3
18		168.73	

Table T-S11: NMR characterisation data for 3c in MeOD.

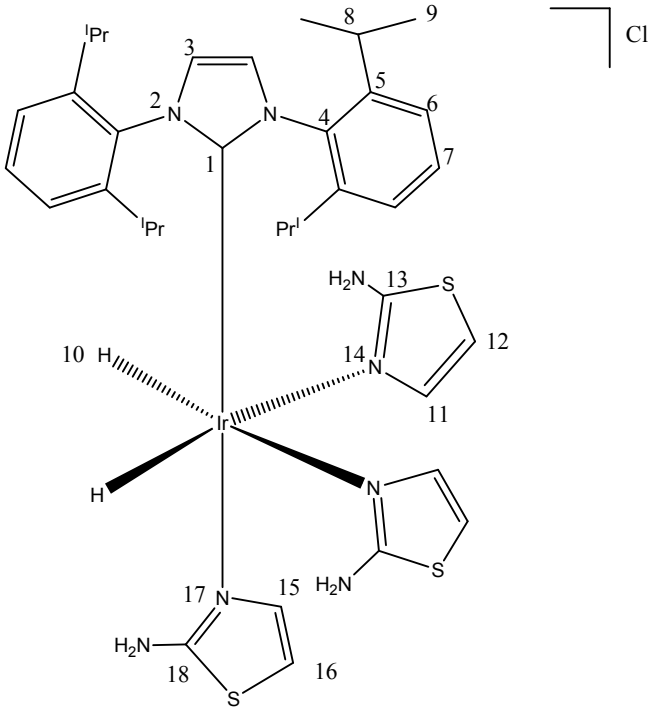

Resonance number	^{1}H (ppm)	^{13}C (ppm)	^{15}N (ppm)
1		153.05	
2			193.6
3	7.405	124.65	
4		128.65	
5		145.99	
6	7.32 (d 8.1 Hz)	123.87	
7	7.49 (t, 8.1 Hz)	129.34	
8	1.21 (d, 7.6 Hz) and 1.14 (d, 7.6 Hz)	20.95, 25.16	
9	2.82 (sept, 7.6 Hz)	28.83	
10	-23.38		
11	7.04 (d 4.1 Hz)	139.79	
12	6.62 (d 4.1 Hz)	105.9	
13		170.48	
14			183.2
15	6.18 (d 4.1 Hz)	137.44	
16	5.44 (d 4.1 Hz)	105.9	
17			168.8
18		169.83	

2.7 Using SABRE to create pseudo singlet states

A typical Shake and Drop (SD) experiment is performed by adding *para*-hydrogen gas into the NMR tube and then shaking it vigorously in a specified magnetic field for around 10 secs before putting the sample into the magnet for immediate signal detection. A hard 90 degree pulse is used to detect the signal in all the SD measurements.

A more controlled measurement was completed using the 'flow' system (see reference for details). Here the full process of gas mixing, transferring and signal detection is completed in conjunction with an automated micro-chip controlled system. The 'Flow' system takes slightly longer for sample transfer and often provides lower SABRE enhancements but it gives much better result precession and reproducibility. A typical result is presented in Figure S9.

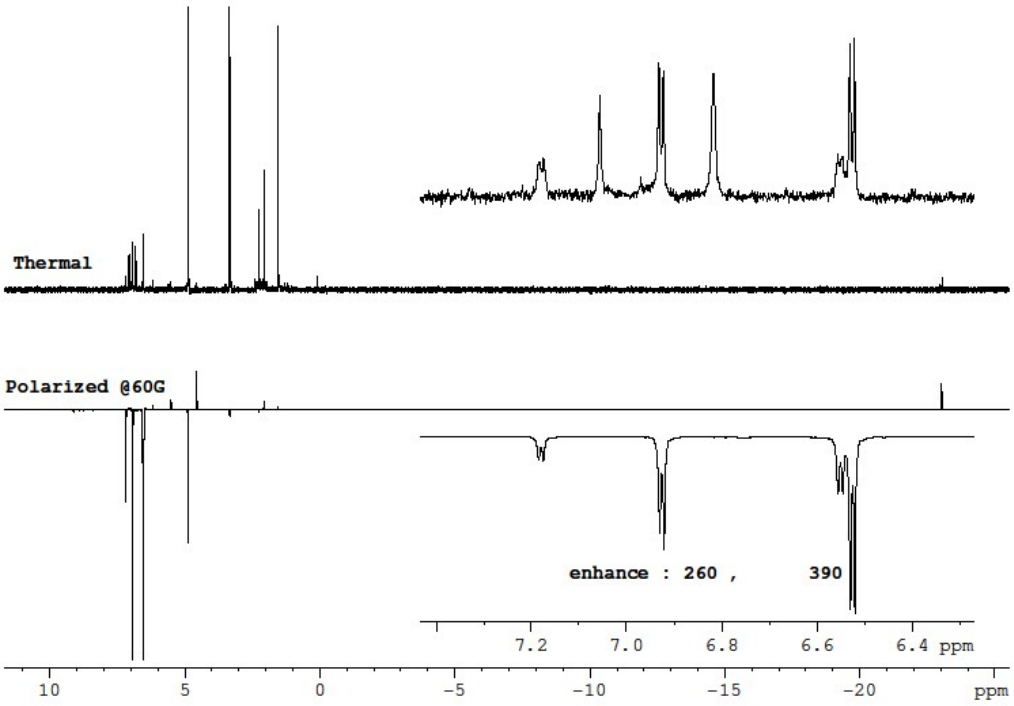

Figure S9: Typical SABRE ^{1}H NMR spectrum, compared to the corresponding thermal trace.

The pseudo singlet states employed here were created by using the pulse sequence of Levitt [14].

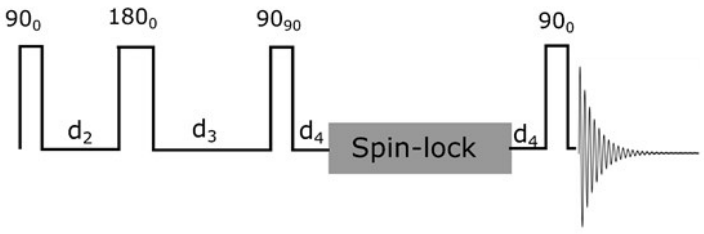

Figure S10. Schematic representation of the pulse sequence used, indicating the type of the pulses employed and the relevant delays that are calculated as a function of the J-coupling and the chemical shift difference between the two spins.

This pulse sequence is suitable for a weakly coupled spin-1/2 pair system. Delays were optimized according to the relative J- coupling (3.8 Hz) and chemical shift (160.8 Hz) values, as follows: d_2 = 65.79 ms, d_3 = 68.91 ms and d_4 = 1.56 ms. The spin-lock was used as a filter to separate out the singlet and to preserve the state. The decay of the singlet state was measured by varying the spin-lock duration from 0 to 120 seconds. Spectra obtained for different durations of the spin-lock pulse are presented below, in Fig. S11, illustrating the decay of the LLS state.

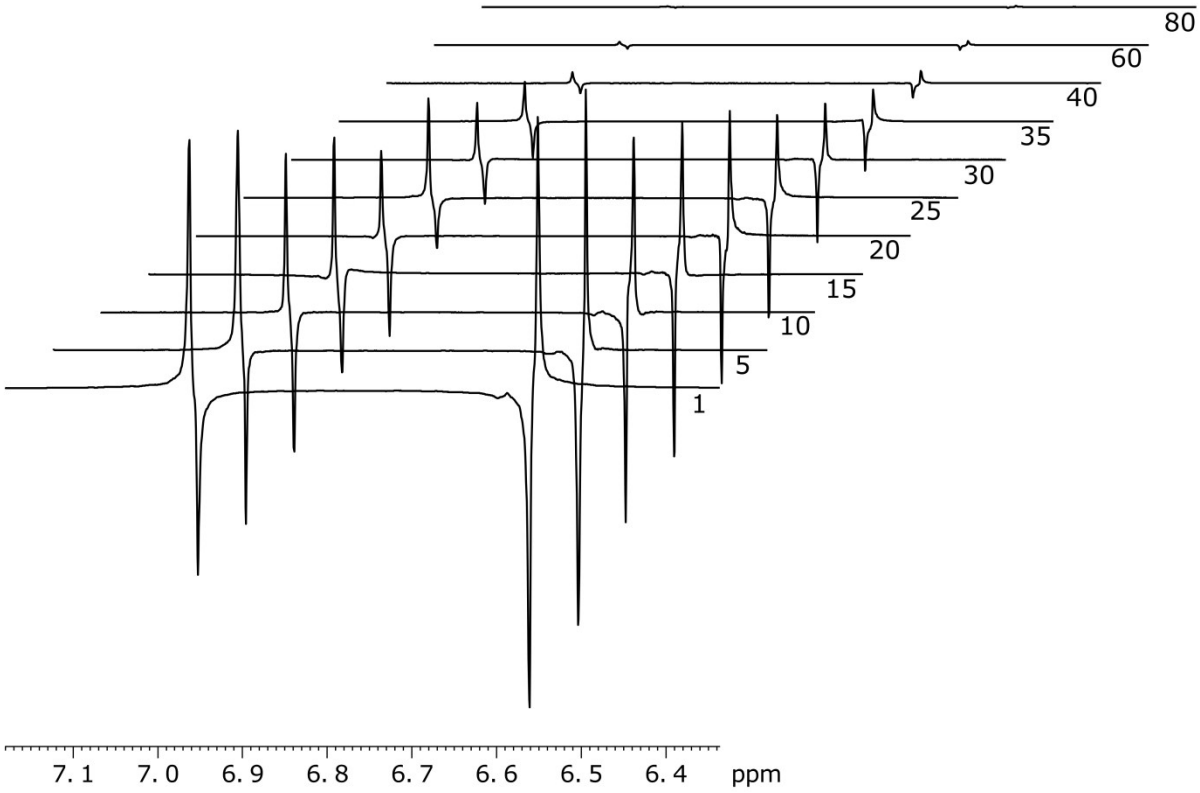

Figure S11. Spectra measured for 3b (5 mM catalyst, 17-fold excess of atz) obtained using the acquisition strategy presented in Fig. S10 and spin-lock pulses of increasing durations (indicated on the right-hand side of the spectra, in s).

Decay curves obtained from the integration of the spectra were plotted against the pulse length and fitted to obtain the values of T_{LLS} (figure S12).

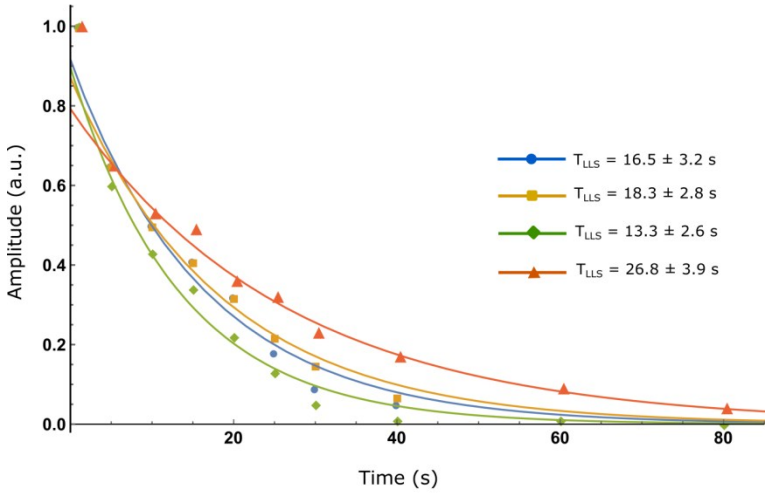

Figure S12. LLS signal amplitude vs. the spin-lock pulse duration for 3a (blue 1:2, yellow 1:17) and 3b (green, 1:2, red 1:17).

As demonstrated, SABRE creates highly polarized longitudinal magnetization of different orders. From this study, the majority of magnetization is 1st order, which is of interest here. For simplicity, we have neglected the two and higher order magnetization terms. The hyperpolarized first order longitudinal magnetization that was created under SABRE was then used as the starting point to create a singlet state by applying the pulse sequence above. The results of this SABRE driven singlet state creation are shown in Fig. 2 of the main draft. The decay pattern clearly shows the long-lived nature of the singlet state, as shown in the main article Fig. 3. A singlet lifetime of 26.8 s was estimated which compares with the T_1 values of 23-26 s for the two individual protons. **3. Theory and simulations**

We used a theoretical approach presented in [14,15] to understand and simulate the current system. The simulations are based on solving the Liouville-von Neumann equation and all the calculations are done using home-developed software in Mathematica [15].

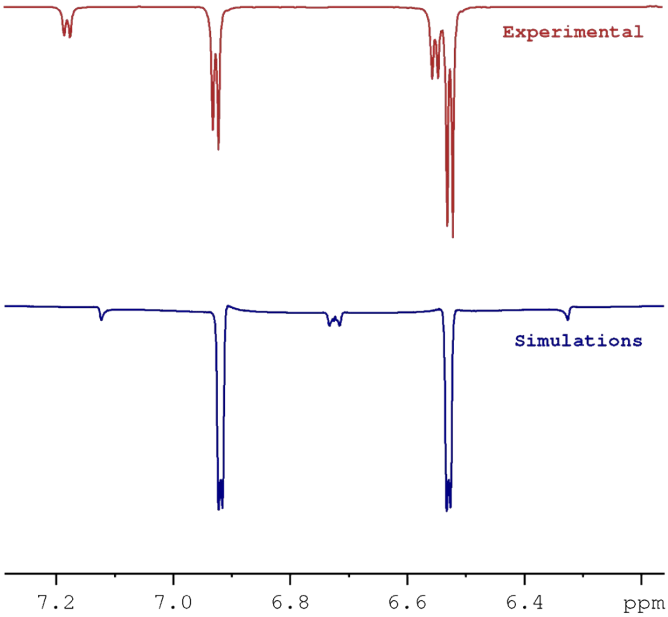

Figure S-13: SABRE enhanced spectra at 60 G by experiment (top trace) and simulations (bottom trace).

The system evolution was modelled in different magnetic fields to get a detailed picture of the spin ensemble and its evolution. In these simulations we assumed our initial state was a pure 'para' state (i.e. singlet). Figure S-11 shows the experimental and simulated SABRE spectra produced after transfer at 60 G. The 'blue' and 'red' lines show the magnetization of the two spins in the system. The maximum signal enhancement theoretically predicted occurs at 50 G, instead of the 60 G estimated experimentally. The overall shape of the field profile matches well however with our experimental results (see Fig. S5). The mismatch can be attributed to the assumption of a pure initial state, and the exchange rates between free and bound substrate.

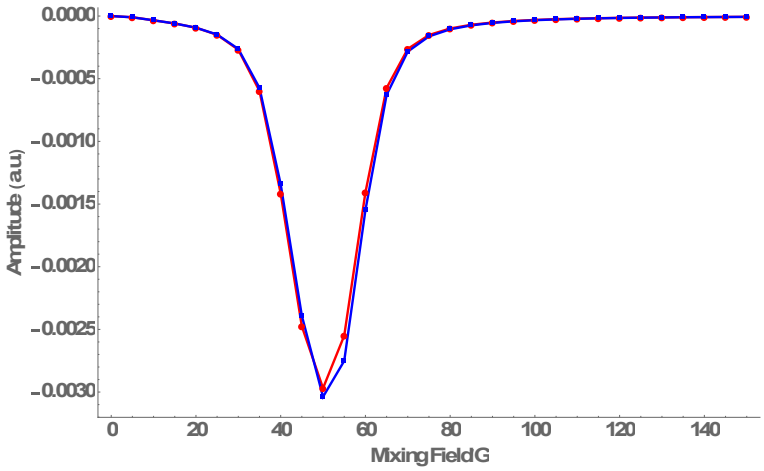

Figure S-14: Simulated field profile plot of SABRE. Red and blue indicates the results for the two distinct spins in the system.

4. References

[1] Torres, O.; Martín, M.; Sola, E. *Organomet.,* 2009, *28*, 863.

[2] L. S. Lloyd, L. S.; Asghar,A.; Burns, M. J.; Charlton, A.; Coombes, S.; Cowley, M.J.; Dear, G. L.; Duckett, S. B.; Genov, G. R.; Green, G. G. R.; Highton, L. A. R.; Hooper, A. J. J.; Khan, M.; Khazal, I. G.; Lewis, R. J.; Mewis, R. E.; Roberts, A. D.; Ruddlesden, A. J., *Catalysis Science & Technology*, 2014, *4*, 3544.

[3] Stott, K.; Stonehouse, J.; Keeler, J.; Hwang, T. L.; Shaka, A. J. *J. Am. Chem. Soc.* 1995, *117*, 4199.

[4] Stonehouse, J.; Adell, P.; Keeler, J.; Shaka, A. J. *J. Am. Chem.,* 1994, *116*, 6037.

[5] Shaw, A. A.; Salaun, C.; Dauphin, J. F.; Ancian, B. *J. Mag. Res. Series A.,* 1996, *120*, 110.

[6] Ancian, B.; Bourgeois, I.; Dauphin, J. F.; Shaw, A. A. *J. Mag. Res.,* 1997,*125*, 348.

[7] Kessler, H.; Oschkinat, H.; Griesinger, C. *J. Mag. Res.,* 1986, *70*, 106.

[8] Vassilev, N. G.; Dimitrov, V. S. *Mag. Res. Chem.,* 2001, *39*, 607.

[9] Mewis, R. E.;, Atkinson, K. D.; Cowley, M. J.; Duckett, S. B.; Green, G. G. R,; L. A. R. Highton, D. Kilgour, L. S. Lloyd, J. A. B. Lohman and D. C. Williamson, *Mag. Res. Chem.*, 2014, *52*, 358.

[10] Jones, W. D.; Rosini, G. P.; Maguire, J. A. *Organomet.,* 1999, *18*, 1754.

[11] (a) C. Runge,*Math. Ann.*, 1895, *46*, 167. (b) W. Kutta, *Z. Math. und Phys.*, 1901, *46,* 435.

[12] (a) Kenneth Levenberg, *Quarterly of Applied Mathematics* 1944, *2*, 164. (b) Donald Marquardt. *Journal on Applied Mathematics,* 1963, ***11*** *(2),* 431.

[13] (a) Eyring, H., *Chem. Rev.*, 1935, *17 (1)*, 65. (b) Polanyi, J. C., *Acc. Chem. Res.*, 1972, *5 (5)*, 161.

[14] Carravetta , M.; Levitt M. H., *J. Am. Chem. Soc*., 2004, *126*, 6228.

[15] Adams, R. W.; Duckett, S. B.; Green, R. A.; Williamson D. C. and Green, G. G. R. *J. Chem. Phys.*, 2009, **131**, 194505.